Accounting for Stimulations That Do Not Elicit Motor-Evoked Potentials When Mapping Cortical Representations of Multiple Muscles

Fang Jin[1,2], Sjoerd M. Bruijn[1,2] and Andreas Daffertshofer[1,2]*

[1] Department of Human Movement Sciences, Faculty of Behavioural and Movement Sciences, Vrije Universiteit Amsterdam, Amsterdam, Netherlands, [2] Faculty of Behavioural and Movement Sciences, Institute Brain and Behavior Amsterdam, Vrije Universiteit Amsterdam, Amsterdam, Netherlands

The representation of muscles in the cortex can be mapped using navigated transcranial magnetic stimulation. The commonly employed measure to quantify the mapping are the center of gravity or the centroid of the region of excitability as well as its size. Determining these measures typically relies only on stimulation points that yield motor-evoked potentials (MEPs); stimulations that do not elicit an MEP, i.e., non-MEP points, are ignored entirely. In this study, we show how incorporating non-MEP points may affect the estimates of the size and centroid of the excitable area in eight hand and forearm muscles after mono-phasic single-pulse TMS. We performed test-retest assessments in twenty participants and estimated the reliability of centroids and sizes of the corresponding areas using inter-class correlation coefficients. For most muscles, the reliability turned out good. As expected, removing the non-MEP points significantly decreased area sizes and area weights, suggesting that conventional approaches that do not account for non-MEP points are likely to overestimate the regions of excitability.

Keywords: TMS, motor evoked potential (MEP), muscle mapping, cortical representation, primary motor cortex (M1)

INTRODUCTION

Single-pulse transcranial magnetic stimulation (TMS) is a non-invasive and painless technique that monitors neurophysiological alterations of the human motor cortex (Barker et al., 1985; Schambra et al., 2003). A TMS coil discharge at suitable intensity will induce transient currents and cause depolarization of axons of nerve cells (Rossini et al., 2015). When applied over the motor cortex, this can elicit a motor-evoked potential (MEP) that can be recorded in contralateral target muscles using conventional electromyography (EMG). Amplitudes and latencies of the MEPs reveal the excitability and conduction times of the cortical-spinal tract. Both have been conceived as valid outcomes of TMS motor mapping (Rossini et al., 1994). Neuroscientists and physicians alike utilized TMS motor mapping to evaluate muscle synergies and motor cortical plasticity (Siebner and Rothwell, 2003), to plan brain tumor surgery (Krieg et al., 2012), or to follow recovery after stroke (Mark et al., 2006; Sondergaard et al., 2021). There is ample evidence that the location at

which TMS elicits the maximum MEP is particularly close to the location found using direct cortical stimulation, which is considered the gold standard in motor mapping. The localization clearly outperforms other modalities like magnetoencephalography (Tarapore et al., 2012) or functional magnetic resonance imaging (Forster et al., 2011).

TMS combined with neuro-navigation increases mapping accuracy (Krieg et al., 2017). A popular approach for coil positioning is a pseudo-random walk. Delivering stimulations at random locations roughly evenly spaced over the motor cortex is more efficient and potentially more accurate than time-consuming, course-grained grid-based positioning. Likely, this random placement will also elicit MEPs in muscles other than the target muscle. Often considered a confounder, this is—in fact—particularly useful when multiple muscles are being evaluated, presuming that the muscles have similar resting motor thresholds (Krieg et al., 2017) and close-by cortical representations (Schieber, 2001). Very recently, Tardelli et al. (2021) used the pseudo-random walk method to assess the cortical representation of abductor digiti minimi, flexor carpi radialis, and flexor pollicis brevis. As a rule of thumb: the more muscles are measured simultaneously, the more efficient assessments *via* pseudo-random coil positioning can be.

Irrespective of the experimental protocol, navigated TMS derived cortical map outcomes should have good reliability (Novikov et al., 2018). Nonetheless, "even most commonly used outcomes such as areas, volumes, the location of centers of gravity (CoGs), and hotspots have (hardly) been validated for being reliable measures in test-retest studies (Kraus and Gharabaghi, 2016)." We slightly modified this quote from Novikov et al. (2018), because they and other likewise recent reports did indeed test for the reliability of navigated TMS outcomes considered in the respective studies. For instance, Nazarova et al. (2021) evaluated the reliability of the CoG and the size of the area (volume) of excitability, next to the position of the MEP hotspot. In a grid-based approach, all measures displayed high relative but low absolute reliability, with the latter arguably reflecting between-subject variability.

The area of excitability can be defined as the cortical region within which TMS elicits an MEP. It is usually determined by projecting the focal point of the coil's magnetic field on a (re-)constructed spherical surface or volume and determining the resulting convex hull. State-of-the-art fine-tuning of this approach is to a priori concentrate on the cortical patch of interest. However, a mapping that agrees with the "real" anatomical structure generally provides better area estimates. This is particularly true when realizing that the gray matter border may have large curvatures along gyral ridges (Van Essen, 2004), where spherical approximations will be poor. We followed these lines and extracted subject-specific cortical surfaces at high resolution, projected the stimulation points to that surface and estimated the area spanned by the pair-wise shortest paths connecting the stimulation points. More importantly, we also projected the stimulation points where TMS did *not* elicit an MEP and removed these points from the estimated area. As will be shown, together these steps circumvent potential over-estimation of the area of excitability.

MATERIALS AND METHODS

Participants

Twenty healthy, right-handed volunteers (average age: 29.6 ± 7.5, eight females) participated in the study. Prior to the experiment, all participants were screened for contraindications of MRI and TMS through questionnaires (Rossi et al., 2011). All of them provided signed informed consent prior to joining the experimental sessions. The Edinburgh Handedness Inventory served to determine hand dominance (Oldfield, 1971). The study had been approved by the medical ethics committee of Amsterdam University Medical Center (VUmc, 018.213–NL65023.029.18).

Materials

Our set-up consisted of three devices: a TMS system, an EMG amplifier, and a neural navigation system. Single-pulse TMS was delivered by a Magstim 200^2 stimulator (Magstim Company Ltd., Whitland, Dyfed, United Kingdom) using a figure-of-eight coil with 70 mm windings. Eight bipolar EMG signals were recorded using a 16-channel EMG amplifier (Porti, TMSi, Oldenzaal, Netherlands) and continuously sampled at a rate of 2 kHz. The EMG recordings were triggered by the TMS to allow for online EMG assessments using a custom-made Labview-program with embedded Matlab functions (designed at our department using Labview 2016, National Instruments, Austin, TX, and Matlab 2018b, The MathWorks, Natick, MA). In brief, upon receiving a trigger, peak-to-peak amplitudes and latencies of MEPs were estimated from all EMG signals during the following 500 ms. These outcomes, as well as the original EMG signals (duration = 500 ms), were sent to the neural navigation system (Neural Navigator, Brain Science Tools, De Bilt, Netherlands)[1] for online monitoring and storage. The neural navigation software also stored the position and orientation of the coil with respect to the head.
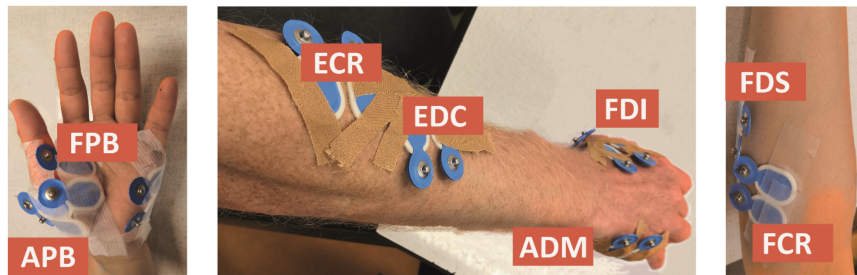
Prior to running the TMS protocol, we acquired the participants' anatomical T1-weighted MRI (3 Tesla Philips Achieva System, Philips, Best, Netherlands; matrix size $256 \times 256 \times 211$, voxel size $1.0 \times 1.0 \times 1.0 \text{ mm}^3$, TR/TE 6.40/2.94 ms). For online neuro-navigation, gray matter was segmented using SPM[2]; note that for offline analysis, we employed a more detailed segmentation *via* Freesurfer.[3]

We considered the first dorsal interosseous (FDI), abductor digiti minimi (ADM), abductor pollicis brevis (APB), flexor pollicis brevis (FPB), extensor digitorum communis (EDC), flexor digitorum superficialis (FDS), extensor carpi radialis (ECR), and flexor carpi radialis (FCR) muscles, which were measured using bipolar electrodes (Blue Sensor N-00-S, Ambu, Ballerup, Denmark), placed after cleaning the skin with alcohol (cf. **Figure 1**). The ground electrode was attached to the ulnar styloid process. We monitored and kept the electrode impedance below 5 kΩ. During the experiment, the orientation of the TMS coil was held 45 degrees to the sagittal plane, and tangential to the

---

[1] www.brainsciencetools.com
[2] https://www.fil.ion.ucl.ac.uk/spm/software/spm12/
[3] https://surfer.nmr.mgh.harvard.edu/fswiki

FIGURE 1 | Electrode placement for the first dorsal interosseous (FDI), abductor digiti minimi (ADM), abductor pollicis brevis (APB), flexor pollicis brevis (FPB), extensor digitorum communis (EDC), flexor digitorum superficialis (FDS), extensor carpi radialis (ECR), and flexor carpi radialis (FCR) muscles.

scalp. By this, we meant to induce currents in the cortex along the posterior-to-anterior direction. To control the TMS output, we used the Matlab-toolbox Rapid2.[4]

Experimental Procedures

Participants were seated comfortably in an armchair, relaxing muscles of hands and arms. The experiment consisted of two identical sessions, *Session 1* and *Session 2*. These sessions were separated by 1h and served to test for test-retest reliability of our outcomes. EMG electrodes were kept fixed to minimize placement errors. The interval of 1h was set to prevent drying of the conductive electrolyte gel.

In each session, we searched for the hotspot positions for FDI, EDC and FCR before testing the RMTs. First, the stimulation intensity was identified that yielded MEPs for all three muscles when stimulating in the omega-shaped area ("hand knob") of the precentral gyrus. We started at 45% of the maximum stimulator output and increased or decreased the intensity until a consistent MEP was present. Then, we performed thirty stimulations around the hand knob region along the precentral gyrus. From these stimulations, we determined the position with the largest peak-to-peak amplitude for every muscle and labeled that position as the hotspot. Next, the RMT for every muscle was determined at the muscle-specific hotspot as the minimum stimulator output at which peak-to-peak amplitudes exceeded 50 µV in five out of ten stimuli. This was followed by the actual mapping procedure.

The TMS coil was pseudo-randomly positioned such that stimulations covered the entire left precentral gyrus. We applied 120 stimulations (Cavaleri et al., 2017) and repeated this at three intensities: 105% RMT of FDI, EDC, and FCR, respectively. In total, we performed 360 stimulations in every session. We chose 105% RMT because previous studies suggested it to be the lowest possible intensity for upper limb muscles mapping (Krieg et al., 2017), thus leading to the least stimulation cross-talk. Finally, we estimated the hotspots of the other five muscles (ADM, APB, FPB, FDS, and ECR) and determined the respective RMTs.

Motor-Evoked Potentials Definition

We discriminated between TMS with and without eliciting MEPs, i.e., MEP and non-MEP points. MEPs were considered proper if their amplitude exceeded 20 times the EMG-baseline's standard deviation (defined over 100 ms prior to each stimulation). While on average these thresholds were [51, 51, 76, 63, 59, 55, 70, and 64] µV for FDI, ADM, APB, FPB, EDC, FDS, ECR, and FCR, respectively, the baseline's standard deviations differed substantially over the group rendering a subject-specific threshold definition appropriate—see **Supplementary Figure 2** for the corresponding boxplots and median values. Amplitudes were also required to stay below 10 mV (to exclude movement and cable artifacts) and the peak's latency had to fall within the range of 5–50 ms after stimulation. All other stimulations were marked as non-MEP points; see below under *Outcome measures* for further details.
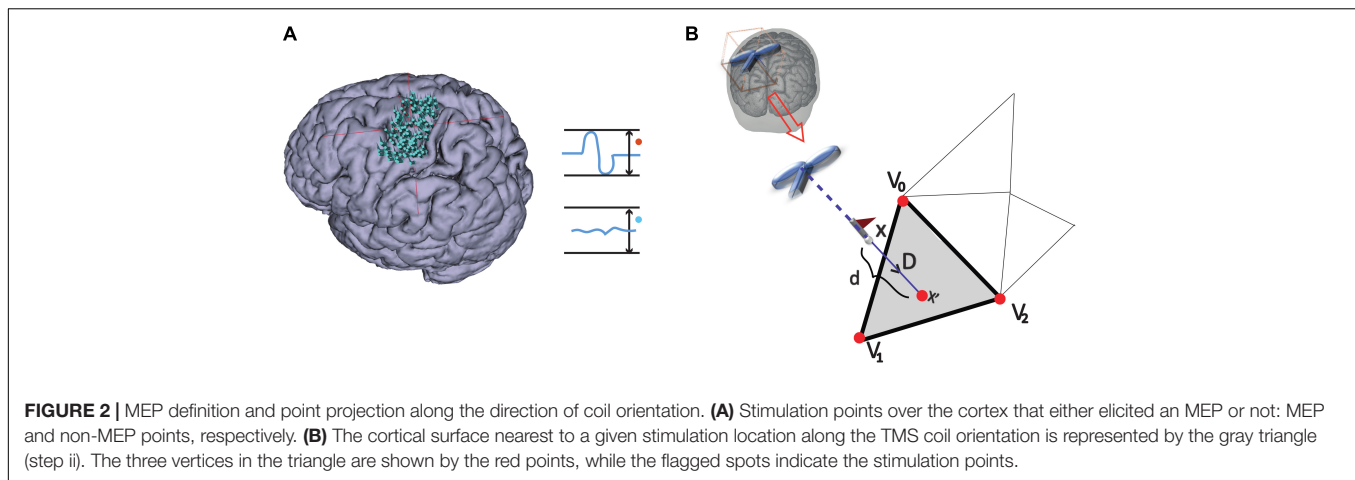
Area Estimate

The area estimates were based on triangulated cortical surface meshes that we extracted using Freesurfer (see text footnote 3; version 7). We imported the meshes into Brainstorm (version 3)[5] to ease converting between world and subject-specific MRI coordinates. Next to the original meshes with about 230,000–340,000 vertices dependent on the participant, we also generated low-resolution version by downsampling the mesh to either 15,000 or 100,000 vertices. This enabled us to test for effects of surface resolution. In all cases, we assigned the Mindboggle anatomical atlas (version 6; see also Klein et al., 2017)[6] to select left primary motor cortex. The area construction consisted of four steps:

(i) Stimulation points were projected to the triangulated cortical surface mesh yielding a set of vertices as illustrated in **Figure 2** and further detailed under *Outcome measures*.

(ii) Vertices that did not fall in left primary motor cortex were excluded (label "precentral L" in the Mindboggle6 atlas).

(iii) We connected the vertices along their shortest connecting paths. In brief, we converted the mesh into a sparse, weighted graph. The edges of triangularization served as adjacencies that we weighted by the Euclidean distance between the corresponding vertices. Then, we searched for the shortest paths between all MEP points (Dijkstra, 1959). We repeated this iteratively for all points of the

---

[4]https://github.com/armanabraham/Rapid2

[5]https://neuroimage.usc.edu/brainstorm/
[6]https://mindboggle.info

FIGURE 2 | MEP definition and point projection along the direction of coil orientation. **(A)** Stimulation points over the cortex that either elicited an MEP or not: MEP and non-MEP points, respectively. **(B)** The cortical surface nearest to a given stimulation location along the TMS coil orientation is represented by the gray triangle (step ii). The three vertices in the triangle are shown by the red points, while the flagged spots indicate the stimulation points.

connecting paths until no points were added. **Figure 3A** briefly summarizes this iteration. Further details can be found at github.[7]

(iv) Finally, we excluded the vertices (and triangles) corresponding to non-MEP points from the resulting area as sketched in **Figure 3B**. Note that if a triangle contained both, one or more stimulations that elicited a MEP and one or more stimulations that did not, we kept the triangle. By this we limited the risk of underestimation that may stem only from falsely considering stimulation points as non-MEP points.

By construction, removing non-MEP points will reduce the size of the active areas. To appreciate the benefits of non-MEP point removal, consider the case in which the true area of excitability has a non-convex boundary, e.g., if the area is U-shaped. Conventional estimates, in particular ones based on estimating the convex hull of the cloud of stimulation points, will clearly provide an overestimate of the excitable area. Rather than opting for non-convex hull estimates, we used a more general approach that also allows for removing points that are scattered across the area spanned by MEP points. We briefly illustrate this in **Figure 4** showing data of a single subject where isolated triangles that are being removed.

From here on, we refer to the reconstruction without accounting for non-MEP points as method M1, whilst the removal of non-MEP points will be method M2 (with examples in **Figures 4A,B**, respectively).

Outcome Measures

Most of the outcome measures were based on the MEP amplitudes and latencies. We quantified them for every TMS pulse and for every muscle using the original EMG signals, from which we removed the stimulation artifact *via* linear interpolation (−1 to +2 ms around stimulation) followed by high pass filtering at 10 Hz (2nd order, bi-directional Butterworth design). We defined the epoch −100 to −1 ms before the stimulus as a baseline and determined its mean value μ and

the standard deviation σ. A peak in the interval 5–100 ms after the stimulus was considered an MEP if its value exceeded μ ± 20σ. Its latency was set as the first sample after the stimulus at which the signal exceeded μ + 2σ (μ − 2σ) if the first peak is a maximum (minimum). Finally, we removed MEPs with peak-to-peak amplitude larger than 10 mV as we considered them artifacts. Except for the latter artifact definition, we opted for relative-to-baseline changes when identifying MEPs to circumvent between-subject variability in skin conductance; the choices for ± 20σ and ± 2σ were based on visually inspecting the EMG traces.
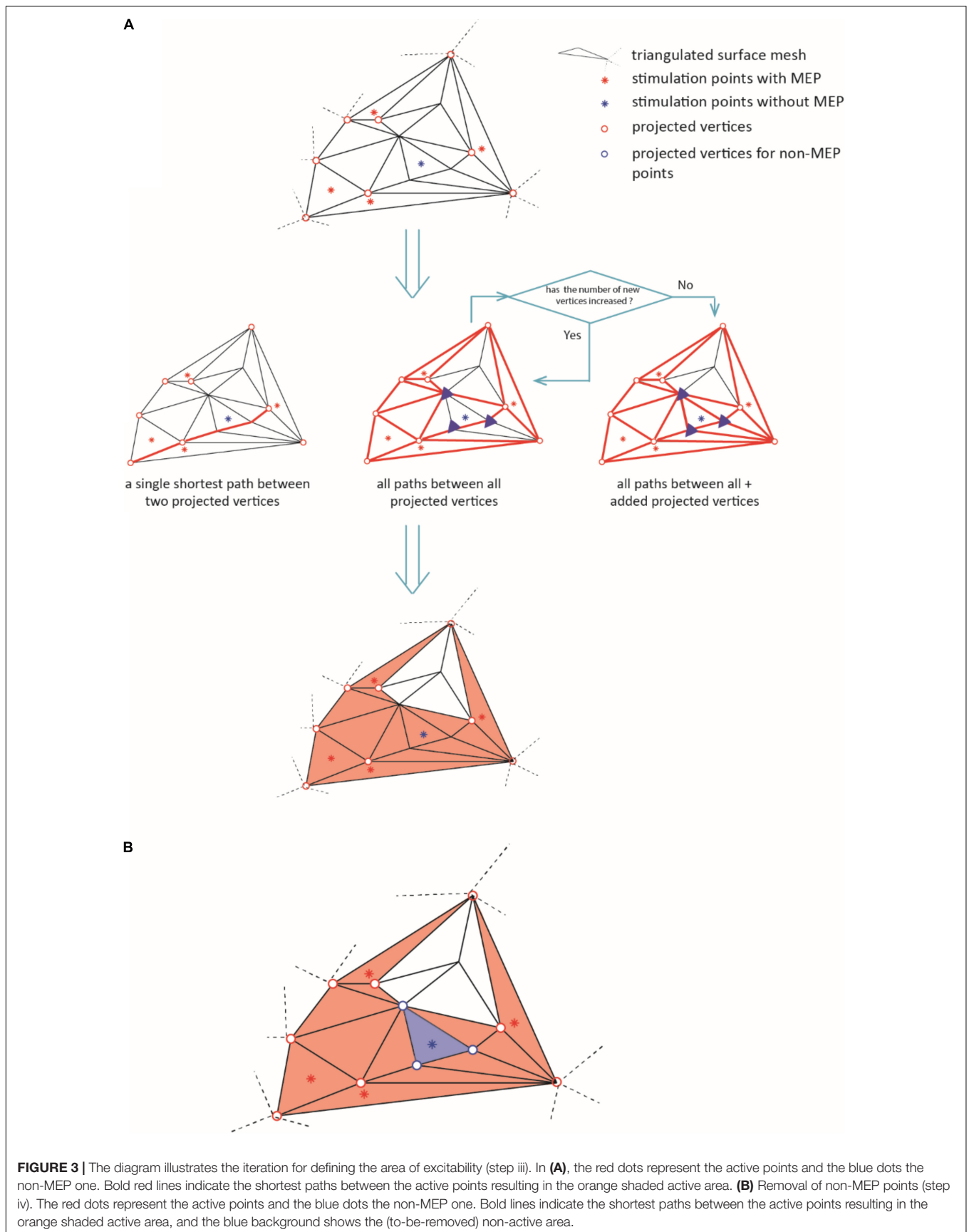
The stimulation points were mapped onto cortical surfaces given as triangulated meshes. The triangle of the surface mesh closest to a stimulation point along the direction of coil orientation was determined following the approach by Möller and Trumbore (1997) (see **Figure 2**). We assigned the vertices $\vec{v}_0$, $\vec{v}_1$, and $\vec{v}_2$ of the closest triangle the corresponding amplitude value, a. If two or more stimulations with an MEP shared a vertex, we averaged their amplitudes at the shared point. Since the total area of excitability possibly covered points that were not projected directly, we set all amplitude values *via* natural interpolation with C^1 continuity to $\hat{a}$; note that if interpolation was not needed, i.e., at the original vertices $\vec{v}_0$, $\vec{v}_1$, and $\vec{v}_2$, then $\hat{a} = a$. For every triangle we defined the length between their vertices as $\lambda_0 = \|\vec{v}_0 - \vec{v}_1\|$, $\lambda_1 = \|\vec{v}_1 - \vec{v}_2\|$ and $\lambda_2 = \|\vec{v}_2 - \vec{v}_0\|$, with $\|\cdots\|$ denoting the Euclidean distance between vertices. That is, given Cartesian coordinates $\vec{v}_i = (x_i, y_i, z_i)$, we used, e.g., $\lambda_0^2 = (x_0 - x_1)^2 + (y_0 - y_1)^2 + (z_0 - z_1)^2$.

The total area A of $k = 1, ..., M$ triangles weighted by the MEP amplitudes was computed *via* a slight modification of Heron's formula, namely the triangular prism, that reads:

$$A = \sum_{k=1}^{M} \overline{a}_k \sqrt{\Lambda_k \left(\Lambda_k - \lambda_{1,k}\right) \left(\Lambda_k - \lambda_{2,k}\right) \left(\Lambda_k - \lambda_{3,k}\right)}$$

with $\Lambda_k = \dfrac{1}{2} \sum_{i=0}^{2} \lambda_{i,k}$ \hfill (1)

FIGURE 3 | The diagram illustrates the iteration for defining the area of excitability (step iii). In **(A)**, the red dots represent the active points and the blue dots the non-MEP one. Bold red lines indicate the shortest paths between the active points resulting in the orange shaded active area. **(B)** Removal of non-MEP points (step iv). The red dots represent the active points and the blue dots the non-MEP one. Bold lines indicate the shortest paths between the active points resulting in the orange shaded active area, and the blue background shows the (to-be-removed) non-active area.

FIGURE 4 | Reconstructed active area in primary motor cortex given a set of stimulation points (orange dots). The color coding indicates the size of the MEP amplitude, with yellow being high and dark red being low. **(A)** Area without removing the non-MEP points (these points are marked in cyan); **(B)** area after removing the non-MEP points. By construction, the area shown in **(B)** is smaller than that in **(A)**. In both cases, the white lines represent an area's boundary; note that this boundary does not necessarily equal the area's convex hull, even when ignoring the non-MEP points **(A)**.

and $\bar{a}_k = \frac{1}{3} \sum_{i=0}^{2} \hat{a}_{i,k}$ being the mean value of (interpolated) MEP amplitudes at the three vertices of triangle k.

Given all $i = 1, ..., N$ area vertices, we further defined the centroid of the total area in line with the conventional form of the center of gravity (Opitz et al., 2014) as:

$$C = \begin{pmatrix} C_x \\ C_y \\ C_z \end{pmatrix} = \frac{1}{\sum_{i=1}^{N} \hat{a}_i} \sum_{i=1}^{N} \hat{a}_i \begin{pmatrix} x_i \\ y_i \\ z_i \end{pmatrix} \quad (2)$$

Statistics

We first estimated the reliability between Session 1 and Session 2 *via* the intraclass correlation coefficients (ICC) of the centroid (C), the weighted area size (A) for every muscle and intensity level. In more detail, we use a two-way mixed-effects model for single measurement type and estimated the absolute agreement, i.e., ICC (2,1) conform the Shrout and Fleiss convention (Koo and Li, 2016). We ran this analysis separately for the three representations of the cortex (i.e., three mesh resolutions) and for the three intensities. While the highest resolution for the intensity of 105% RMT of FCR will be reported below, all the other results can be found as **Supplementary Material**. There we also report the ICCs for centers of gravity (*CoG*) and for both the MEP amplitudes and the latencies.

To further confirm the absence of significant differences between Sessions 1 and 2, we performed a two-way ANOVA with repeated measures including factors of *intensity* and *session*. This also allowed for assessing effects of stimulation intensity. We applied a Bonferroni correction for multiple comparisons. Again, we restrict ourselves to reporting "only" the findings of the estimates at maximum resolution in the body text and refer to **Supplementary Material** for all other cases.

Finally, to assess effects of cortex mesh resolution and of ignoring/removing non-MEP stimulation points, we used a two-way repeated ANOVA with factors *method* and *resolution* (again with Bonferroni correction for multiple comparisons).

Prior to conducting the ANOVAs, sphericity was verified *via* Mauchly's test. A Greenhouse-Geisser correction was performed if necessary. Throughout hypothesis testing, we used

a significance threshold of $\alpha = 0.05$. All statistical analyses were conducted using Matlab (The Mathworks Inc., Natwick MA, version 2020b).

RESULTS

All $N = 20$ participants completed the experimental procedure without adverse reactions. Of all mappings (subjects × muscle × intensity × session = 960, each containing 120 stimulations) 2% did not contain any valid MEP, and thus did not enter further analyses. In 11/320 (subjects × muscles × session) cases this was for 105% RMT of FDI, 5/320 for 105% RMT of EDC, and 1/320 for 105% RMT of FCR; see **Supplementary Table 1**). For five subjects, we could not detect any MEPs for ADM when using the second intensity in both sessions.

When averaged over participants and sessions, the RMTs were FDI: $44.90 \pm 1.46\%$, ADM: $47.90 \pm 1.64\%$, APB: $46.15 \pm 1.45\%$, FPB: $46.78 \pm 1.73\%$, EDC: $45.28 \pm 1.50\%$, FDS: $47.75 \pm 1.51\%$, ECR: $46.55 \pm 1.50\%$, and FCR: $48.00 \pm 1.52\%$, when expressed in stimulator intensity.

Table 1 provides an overview of ICC with the values obtained for maximum cortical resolution (results of the other resolutions and intensities can be found as **Supplementary Tables 2A–C**). For the sake of legibility, we defined distinct classes as follows: excellent: $0.8 \leq$ ICC, good: $0.65 \leq$ ICC < 0.8, moderate: $0.5 \leq$ ICC < 0.65 and poor: ICC < 0.5 (Cavaleri et al., 2018), and color-coded the table entries accordingly.

The ICCs appeared consistent between methods M1 (ignoring non-MEP points) and M2 (removing non-MEP points). Most of them were moderate to good. Good-excellent reliability was found for estimated centroids in the anterior/posterior and superior/inferior directions (x and z coordinates, respectively). While the area sizes' ICCs of FDI, FDS, and FCR were poor, the ANOVA did not reveal any significant differences between the area estimates between sessions. We illustrate this in **Table 2** for the highest cortex resolution and refer to **Supplementary Tables 3A,B** for the ANOVA results for the other cortex

TABLE 1 | ICC values of area sizes A and centroids $C = (C_x, C_y, C_z)^T$ estimated for intensity of 105% RMT of FCR using the cortical meshes with maximum resolution when ignoring non-MEP points (M1) or removing them (M2)*.

	FDI		ADM		APB		FPB		EDC		FDS		ECR		FCR	
	M1	M2	M1	M2	M1	M2	M1	M2	M1	M2	M1	M2	M1	M2	M1	M2
A	0.41	0.42	0.67	0.67	0.55	0.55	0.69	0.69	0.73	0.72	0.32	0.31	0.58	0.57	0.15	0.14
C_x	0.90	0.90	0.88	0.88	0.89	0.89	0.89	0.89	0.92	0.92	0.89	0.89	0.92	0.92	0.91	0.91
C_y	0.58	0.59	0.55	0.55	0.69	0.70	0.61	0.61	0.56	0.57	0.51	0.51	0.51	0.51	0.53	0.53
C_z	0.80	0.80	0.68	0.68	0.76	0.76	0.81	0.82	0.76	0.76	0.66	0.66	0.72	0.72	0.83	0.83

*Excellent: $0.8 \leq ICC$ (dark green, bold); good: $0.65 \leq ICC < 0.8$ (light green); moderate: $0.5 \leq ICC < 0.65$ (yellow); poor: $ICC < 0.5$ (light red).

TABLE 2 | Outcomes of the two-way ANOVA for the area sizes A (in $mm^2 \cdot \mu V \cdot 10^5$) with factors of *intensity* and *session* when considering the highest cortex mesh resolution and when removing the non-MEP points (M2)*.

	⟨A⟩ at 105% RMT			Intensity		Session		Intensity × session		p-value pairwise comparison		
	FDI	EDC	FCR	F	p	F	p	F	p	FDI/EDC	FDI/FCR	EDC/FCR
FDI	1.61 ± 0.24	2.48 ± 0.60	4.86 ± 1.41	F(2, 36) = 4.855	0.032	F(1, 18) = 1.390	0.254	F(2, 36) = 0.634	0.454	0.307	0.087	0.195
ADM	0.92 ± 0.21	0.99 ± 0.17	2.16 ± 0.60	F(2, 24) = 5.385	0.032	F(1, 12) = 1.216	0.292	F(2, 24) = 0.238	0.790	1.00	0.076	0.137
APB	1.63 ± 0.41	1.89 ± 0.45	3.74 ± 1.28	F(2, 34) = 3.050	0.093	F(1, 17) = 0.939	0.346	F(2, 34) = 1.337	0.267	1.00	0.213	0.364
FPB	1.18 ± 0.28	1.53 ± 0.37	2.41 ± 0.69	F(2, 34) = 3.439	0.073	F(1, 17) = 4.425	0.051	F(2, 34) = 1.398	0.260	0.273	0.158	0.406
EDC	1.01 ± 0.21	0.94 ± 0.12	1.75 ± 0.36	F(2, 34) = 5.960	0.016	F(1, 17) = 0.082	0.778	F(2, 34) = 0.146	0.865	1.00	**0.031**	0.078
FDS	0.83 ± 0.12	0.97 ± 0.18	1.60 ± 0.25	F(2, 30) = 6.345	0.005	F(1,15) = 1.090	0.313	F(2, 30) = 1.174	0.323	1.00	**0.020**	0.077
ECR	1.24 ± 0.20	1.62 ± 0.43	2.45 ± 0.53	F(2, 30) = 4.730	0.016	F(1, 15) = 0.319	0.580	F(2, 30) = 0.867	0.388	0.947	**0.030**	0.217
FCR	0.69 ± 0.11	0.99 ± 0.20	1.39 ± 0.20	F(2, 30) = 5.173	0.012	F(1, 15) = 2.079	0.170	F(2, 30) = 1.388	0.265	0.473	**0.011**	0.376

*Bold face implies $p < 0.05$.

TABLE 3 | The outcome of the two-way ANOVA for the area sizes A (in $mm^2 \cdot \mu V \cdot 10^5$) with factors of *method* and *resolution* for the intensity of 105% RMT of FCR; M1, ignoring non-MEP points, M2, removing them*.

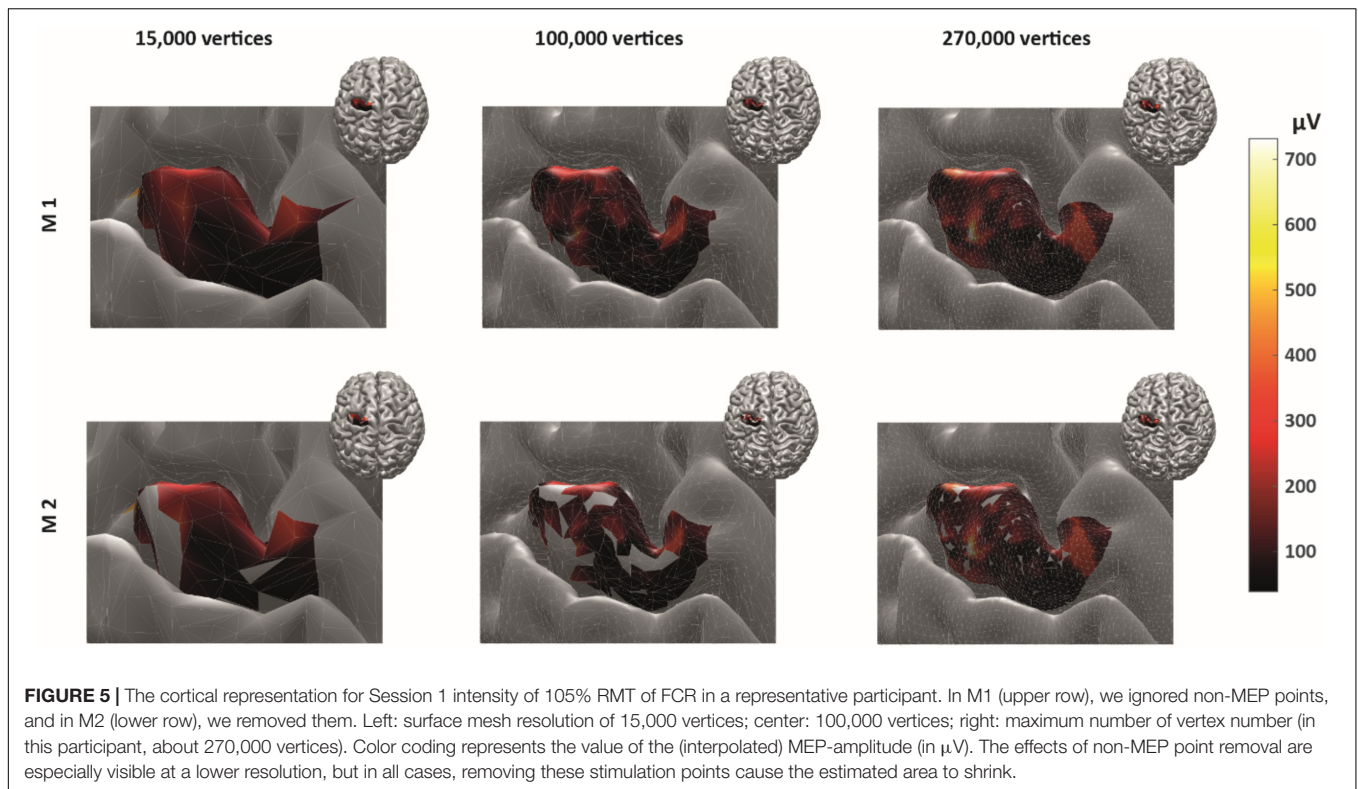|	⟨A⟩ at 105% RMT of FCR		Method		Resolution		Method × resolution	
	M1	M2	F	p	F	p	F	p
FDI	4.81 ± 1.48	4.27 ± 1.25	F(1, 19) = 5.335	0.032	F(2, 38) = 1.655	0.212	F(2, 38) = 3.128	0.093
ADM	1.68 ± 0.50	1.50 ± 0.43	F(1, 17) = 5.158	0.036	F(2, 34) = 1.927	0.173	F(2, 34) = 2.638	0.122
APB	3.54 ± 1.12	3.25 ± 1.03	F(1, 19) = 7.967	0.011	F(2, 38) = 1.002	0.342	F(2, 38) = 3.404	0.079
FPB	2.21 ± 0.59	2.00 ± 0.53	F(1, 19) = 9.775	0.006	F(2, 38) = 1.286	0.273	F(1, 19) = 9.775	**0.006**
EDC	1.63 ± 0.33	1.49 ± 0.29	F(1, 19) = 19.435	0.000	F(2, 38) = 2.625	0.086	F(1, 19) = 19.435	**0.000**
FDS	1.40 ± 0.22	1.29 ± 0.20	F(1, 19) = 24.526	0.000	F(2, 38) = 0.582	0.517	F(2, 38) = 11.278	**0.002**
ECR	2.09 ± 0.43	1.93 ± 0.39	F(1, 19) = 13.025	0.002	F(2, 38) = 2.576	0.089	F(2, 38) = 5.639	**0.023**
FCR	1.43 ± 0.19	1.33 ± 0.17	F(1, 17) = 20.599	0.000	F(2, 34) = 0.096	0.830	F(2, 34) = 9.791	**0.004**

*Bold face implies $p < 0.05$.

resolutions. In **Supplementary Tables 4–6A–C**, we also provide the results for the corresponding centroid positions. In a nutshell there were hardly any significant effects of session or intensity (let alone their interaction) on the centroids; when correcting for multiple comparisons all effects will turn out not significant.

Here we would like to note that this dependency on stimulation intensity can be understood when looking at the effects of intensity on the mere MEP amplitudes, i.e., without projecting them onto the cortex. The corresponding results can be found as **Supplementary Table 7**. In a nutshell, the amplitudes of FDI, EDC, FCR, FDS, and FCR significantly increased with increasing stimulation intensity.

As expected, ignoring non-MEP points (M1) consistently resulted in larger area sizes when compared to the case when non-MEP points were removed (M2). Our second ANOVA confirmed this. We summarized this in **Table 3** where we highlighted the main effects of *method*. Yet, we also would like to note the interaction effect with *resolution*, suggesting that the correction for non-MEP points is especially relevant when incorporating low-resolution cortical meshes (see also **Figure 5**, upper row).

The main effect of *method* (ignoring non-MEPs vs. removing them) is also illustrated in **Figure 6** where we show the relative change in the estimated area sizes. Irrespective of resolution, not removing the non-MEP points yields an overestimation of the

FIGURE 5 | The cortical representation for Session 1 intensity of 105% RMT of FCR in a representative participant. In M1 (upper row), we ignored non-MEP points, and in M2 (lower row), we removed them. Left: surface mesh resolution of 15,000 vertices; center: 100,000 vertices; right: maximum number of vertex number (in this participant, about 270,000 vertices). Color coding represents the value of the (interpolated) MEP-amplitude (in µV). The effects of non-MEP point removal are especially visible at a lower resolution, but in all cases, removing these stimulation points cause the estimated area to shrink.

active areas, though this effect appears particularly pronounced at low resolution (top panel in **Figure 6**).

We finally illustrate the effect of removing non-MEP points in **Figure 5**, where it can be clearly seen that higher resolutions lead to less area being removed.
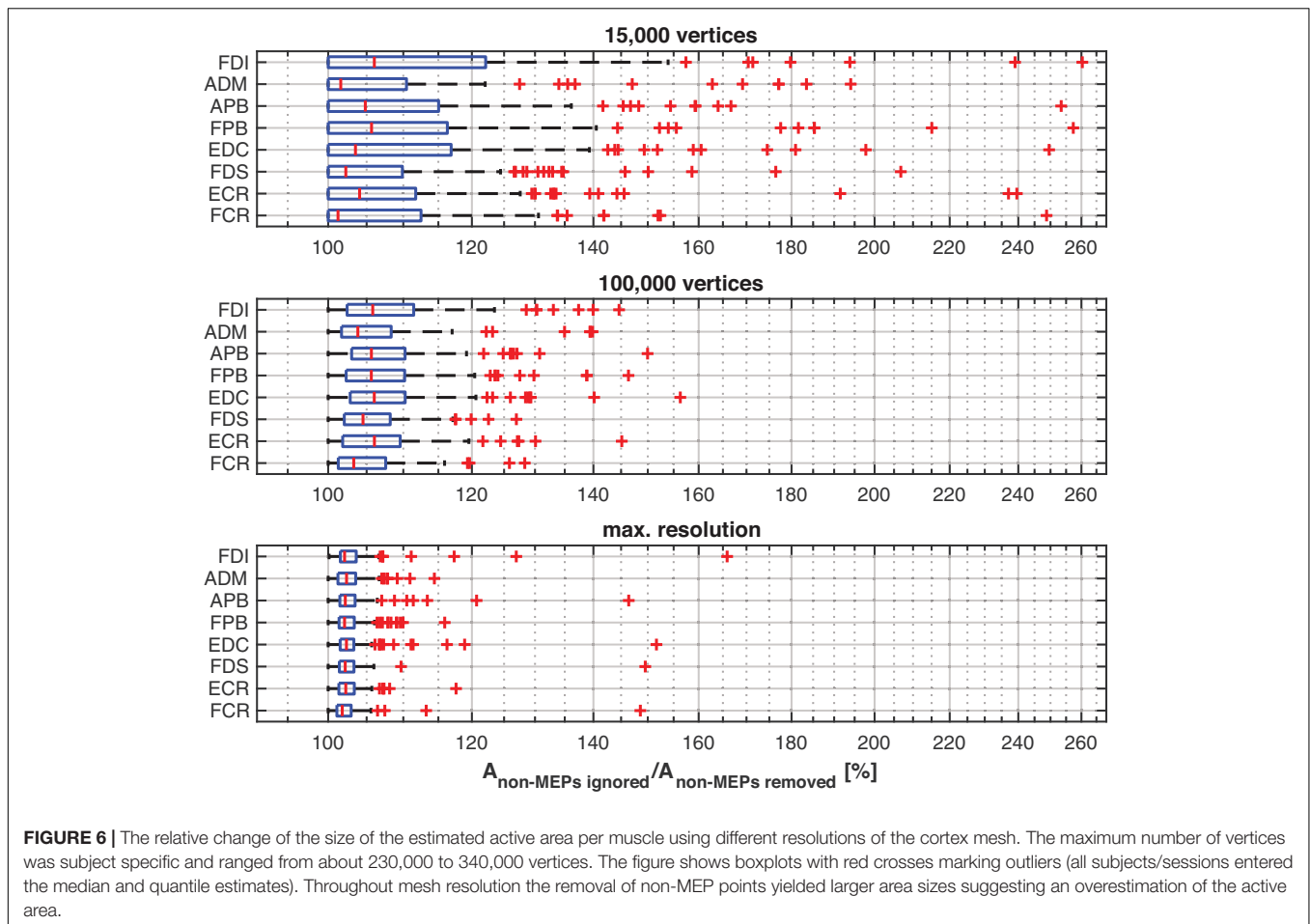
DISCUSSION

We assessed the reliability of the cortical representation of eight muscles mapped simultaneously using navigated TMS. We distinguished two methods to estimate the active area of a muscle. In the first, more conventional one (M1), we included all stimulation points that elicited an MEP. In the second method (M2), we included the same points but also excluded all stimulation points that did not elicit an MEP. We tested for the effects of the type of measure with the obvious expectation that the latter will yield smaller active areas. We also tested for effects of stimulation intensity and cortical mesh resolution in two consecutive sessions. By and large, we found that the reliabilities of the size and the centroids of the active areas for all the muscles were excellent, good, or moderate. Exceptions were the area size estimates in three muscles (**Table 1**) that came with small areas sizes but strong outliers when looking at their representation at high-resolution cortical surface meshes (**Figure 6**, lower panel). The ICCs of amplitude and latency were excellent or good for all the muscles, again supporting the reliability of our experimental approach (cf. **Supplementary Table 8**).

One must realize that designing multiple muscle mapping experiments can—in general—be problematic as the RMT of

a single muscle must be considered a reference when setting the stimulation intensity. In our case, the difference of RMTs values between different stimulation intensities was small (on average 3.1% of stimulator output; when looking at the individual subjects we found maximum differences of $|\mathrm{RMT_{FDI}}\text{-}\mathrm{RMT_{EDC}}|$ = $|\mathrm{RMT_{FCR}}\text{-}\mathrm{RMT_{EDC}}|$ = 9%, and $|\mathrm{RMT_{FDI}}\text{-}\mathrm{RMT_{FCR}}|$ = 8%). Intensities of 105%, 110–120% (Akiyama et al., 2006) RMT have been widely used in motor mapping (Bohning et al., 2001; Akiyama et al., 2006; Tarapore et al., 2012), suggesting that the here-observed difference is acceptable if not negligible. Hence, forearm and hand muscles might be pooled in a group of muscles with "similar RMTs" and may be evaluated at the same intensity.

For all the muscles, the ICCs of the centroids' positions were moderate to excellent. In the **Supplementary Tables 2A–C** we show the likewise good results for the more conventional CoGs. Both the estimated centroid as well as the centers-of-gravity hence appeared very consistent and should be considered reliable outcomes in motor mapping, in particular also the anterior/posterior and superior/inferior directions, in line with previous studies (Weiss et al., 2013; Cavaleri et al., 2018). The CoG is commonly employed to quantify the cortical representation of muscles (Massé-Alarie et al., 2017; Nazarova et al., 2021). However, there are several issues with the notion of "CoG" itself. For instance, for many shapes (of cortical representations), the CoG will lie outside the actual stimulation area itself (consider a banana, whose CoG will not be inside the banana itself). The CoG may hence be a tricky measure to give an estimate of the cortical representation of a muscle, especially when the true cortical representation is non-trivially shaped and on a curved surface. Supplementing the CoG, or in our case the

FIGURE 6 | The relative change of the size of the estimated active area per muscle using different resolutions of the cortex mesh. The maximum number of vertices was subject specific and ranged from about 230,000 to 340,000 vertices. The figure shows boxplots with red crosses marking outliers (all subjects/sessions entered the median and quantile estimates). Throughout mesh resolution the removal of non-MEP points yielded larger area sizes suggesting an overestimation of the active area.

centroid, by the area of excitability is clearly needed, especially when the area estimate is weighted by the MEP amplitude. Again, we advocate incorporating the non-MEP stimulation points in these estimates.

When removing non-MEP points, the areas of excitability became significantly smaller than when non-MEP points were simply ignored. We argue that by ignoring the stimulation points that do not elicit MEPs one runs the risk of overestimating the area of excitability and thus to mis-represent muscles in the cortex. Our results show that accounting for non-MEP points does not jeopardize the reliability of assessments. As such we advocate for correcting any potential structural error and provide the tools to do so. Of course, one may counter the fear for structural errors by subsuming that the neuronal population that ought to be covered by our cortical map are likely to be homogeneously distributed. However, several invasive studies already speak against this (e.g., Schieber, 2001). By using intracortical micro-stimulation, Nudo et al. (1996) revealed that the cortical representation of distal forelimb muscles is quite complicated and clearly not uniform. Moreover, to date most area measures rely on estimating convex hulls that clear yield weak approximations if the excitable area has a non-convex boundary—when looking at precentral gyrus that might be the rule rather than the exception.

CONCLUSION

Estimating the active area can be improved when incorporation points at which TMS does not elicit an MEP. Navigated TMS and a pseudo-random coil placement allow for correcting area estimates post-hoc and hence reduce the risk of overestimating the cortical representation of active areas. As such, the very fact that at certain points, a stimulation does not yield a measurable response appears informative. And, even when assessing multiple muscles in unison, this approach comes with high reliability, albeit under the provison that stimulation intensity has been chosen properly.

DATA AVAILABILITY STATEMENT

The raw data supporting the conclusions of this article will be made available by the authors, without undue reservation.

ETHICS STATEMENT

The studies involving human participants were reviewed and approved by the Medisch Ethische Toetsingscommissie VUmc.

The patients/participants provided their written informed consent to participate in this study. Written informed consent was obtained from the individual(s) for the publication of any potentially identifiable images or data included in this article.

AUTHOR CONTRIBUTIONS

SUPPLEMENTARY MATERIAL

The Supplementary Material for this article can be found online at: https://www.frontiersin.org/articles/10.3389/fnhum.2022.920538/full#supplementary-material

REFERENCES

Akiyama, T., Ohira, T., Kawase, T., and Kato, T. (2006). TMS orientation for NIRS-functional motor mapping. *Brain Topogr.* 19, 1–9. doi: 10.1007/s10548-006-0007-9

Barker, A. T., Jalinous, R., and Freeston, I. L. (1985). Non-invasive magnetic stimulation of human motor cortex. *Lancet* 325, 1106–1107. doi: 10.1016/s0140-6736(85)92413-4

Bohning, D., He, L., George, M., and Epstein, C. (2001). Deconvolution of transcranial magnetic stimulation (TMS) maps. *J. Neural Transm.* 108, 35–52. doi: 10.1007/s007020170095

Cavaleri, R., Schabrun, S. M., and Chipchase, L. S. (2017). The number of stimuli required to reliably assess corticomotor excitability and primary motor cortical representations using transcranial magnetic stimulation (TMS): a systematic review and meta-analysis. *Syst. Rev.* 6, 1–11.

Cavaleri, R., Schabrun, S. M., and Chipchase, L. S. (2018). The reliability and validity of rapid transcranial magnetic stimulation mapping. *Brain Stimul.* 11, 1291–1295. doi: 10.1016/j.brs.2018.07.043

Dijkstra, E. W. (1959). A note on two problems in connexion with graphs. *Numer. Math.* 1, 269–271.

Forster, M.-T., Hattingen, E., Senft, C., Gasser, T., Seifert, V., and Szelényi, A. (2011). Navigated transcranial magnetic stimulation and functional magnetic resonance imaging: advanced adjuncts in preoperative planning for central region tumors. *Neurosurgery* 68, 1317–1325.

Klein, A., Ghosh, S. S., Bao, F. S., Giard, J., Häme, Y., Stavsky, E., et al. (2017). Mindboggling morphometry of human brains. *PLoS Comput. Biol.* 13:e1005350. doi: 10.1371/journal.pcbi.1005350

Koo, T. K., and Li, M. Y. (2016). A guideline of selecting and reporting intraclass correlation coefficients for reliability research. *J. Chiropr. Med.* 15, 155–163.

Kraus, D., and Gharabaghi, A. (2016). Neuromuscular plasticity: disentangling stable and variable motor maps in the human sensorimotor cortex. *Neural Plast.* 2016:7365609. doi: 10.1155/2016/7365609

Krieg, S. M., Lioumis, P., Mäkelä, J. P., Wilenius, J., Karhu, J., Hannula, H., et al. (2017). Protocol for motor and language mapping by navigated TMS in patients and healthy volunteers. workshop report. *Acta Neurochirurgica* 159, 1187–1195. doi: 10.1007/s00701-017-3187-z

Krieg, S. M., Shiban, E., Buchmann, N., Gempt, J., Foerschler, A., Meyer, B., et al. (2012). Utility of presurgical navigated transcranial magnetic brain stimulation for the resection of tumors in eloquent motor areas. *J. Neurosurg.* 116, 994–1001. doi: 10.3171/2011.12.JNS111524

Mark, V., Taub, E., and Morris, D. (2006). Neuroplasticity and constraint-induced movement therapy. *Eura. Medicophys.* 42:269.

Massé-Alarie, H., Bergin, M. J., Schneider, C., Schabrun, S., and Hodges, P. W. (2017). "Discrete peaks" of excitability and map overlap reveal task-specific organization of primary motor cortex for control of human forearm muscles. *Hum. Brain Mapp.* 38, 6118–6132. doi: 10.1002/hbm.23816

Möller, T., and Trumbore, B. (1997). Fast, minimum storage ray-triangle intersection. *J. Graphics Tools* 2, 21–28.

Nazarova, M., Novikov, P., Ivanina, E., Kozlova, K., Dobrynina, L., and Nikulin, V. V. (2021). Mapping of multiple muscles with transcranial magnetic stimulation: absolute and relative test–retest reliability. *Hum. Brain Mapp.* 42, 2508–2528. doi: 10.1002/hbm.25383

Novikov, P. A., Nazarova, M. A., and Nikulin, V. V. (2018). TMSmap-software for quantitative analysis of TMS mapping results. *Front. Hum. Neurosci.* 12:239. doi: 10.3389/fnhum.2018.00239

Nudo, R. J., Milliken, G. W., Jenkins, W. M., and Merzenich, M. M. (1996). Use-dependent alterations of movement representations in primary motor cortex of adult squirrel monkeys. *J. Neurosci.* 16, 785–807. doi: 10.1523/JNEUROSCI.16-02-00785.1996

Oldfield, R. C. (1971). The assessment and analysis of handedness: the Edinburgh inventory. *Neuropsychologia* 9, 97–113. doi: 10.1016/0028-3932(71)90067-4

Opitz, A., Zafar, N., Bockermann, V., Rohde, V., and Paulus, W. (2014). Validating computationally predicted TMS stimulation areas using direct electrical stimulation in patients with brain tumors near precentral regions. *NeuroImage Clin.* 4, 500–507. doi: 10.1016/j.nicl.2014.03.004

Rossi, S., Hallett, M., Rossini, P. M., and Pascual-Leone, A. (2011). Screening questionnaire before TMS: an update. *Clin. Neurophysiol.* 122:1686. doi: 10.1016/j.clinph.2010.12.037

Rossini, P. M., Barker, A., Berardelli, A., Caramia, M., Caruso, G., Cracco, R., et al. (1994). Non-invasive electrical and magnetic stimulation of the brain, spinal cord and roots: basic principles and procedures for routine clinical application. Report of an IFCN committee. *Electroencephalogr. Clin. Neurophysiol.* 91, 79–92. doi: 10.1016/0013-4694(94)90029-9

Rossini, P. M., Burke, D., Chen, R., Cohen, L., Daskalakis, Z., Di Iorio, R., et al. (2015). Non-invasive electrical and magnetic stimulation of the brain, spinal cord, roots and peripheral nerves: basic principles and procedures for routine clinical and research application. An updated report from an IFCN Committee. *Clin. Neurophysiol.* 126, 1071–1107. doi: 10.1016/j.clinph.2015.02.001

Schambra, H., Sawaki, L., and Cohen, L. (2003). Modulation of excitability of human motor cortex (M1) by 1 Hz transcranial magnetic stimulation of the contralateral M1. *Clin. Neurophysiol.* 114, 130–133. doi: 10.1016/s1388-2457(02)00342-5

Schieber, M. H. (2001). Constraints on somatotopic organization in the primary motor cortex. *J. Neurophysiol.* 86, 2125–2143. doi: 10.1152/jn.2001.86.5.2125

Siebner, H., and Rothwell, J. (2003). Transcranial magnetic stimulation: new insights into representational cortical plasticity. *Exp. Brain Res.* 148, 1–16. doi: 10.1007/s00221-002-1234-2

Sondergaard, R. E., Martino, D., Kiss, Z. H., and Condliffe, E. G. (2021). TMS motor mapping methodology and reliability: a structured review. *Front. Neurosci.* 15:709368. doi: 10.3389/fnins.2021.709368

Tarapore, P. E., Tate, M. C., Findlay, A. M., Honma, S. M., Mizuiri, D., Berger, M. S., et al. (2012). Preoperative multimodal motor mapping: a comparison of magnetoencephalography imaging, navigated transcranial magnetic stimulation, and direct cortical stimulation. *J. Neurosurg.* 117, 354–362. doi: 10.3171/2012.5.JNS112124

Tardelli, G. P., Souza, V. H., Matsuda, R. H., Garcia, M. A. C., Novikov, P., Nazarova, M., et al. (2021). Forearm and hand muscles exhibit high coactivation and overlapping of cortical motor representations. *Biorxiv[preprint]* doi: 10.1007/s10548-022-00893-1

Van Essen, D. C. (2004). Surface-based approaches to spatial localization and registration in primate cerebral cortex. *NeuroImage* 23, S97–S107. doi: 10.1016/j.neuroimage.2004.07.024

Weiss, C., Nettekoven, C., Rehme, A. K., Neuschmelting, V., Eisenbeis, A., Goldbrunner, R., et al. (2013). Mapping the hand, foot and face representations in the primary motor cortex – retest reliability of neuronavigated TMS versus functional MRI. *NeuroImage* 66, 531–542. doi: 10.1016/j.neuroimage.2012.10.046